ANNALS OF GEOPHYSICS, 68, 1, V101, 2025; doi:10.4401/ag-9152
OPEN ACCESS

Volcano-tectonic seismicity and related hazard: a component of the multi-hazard assessment in the highly exposed region of Mt. Etna (Italy)

Salvatore D'Amico[*,1], Raffaele Azzaro[1], Giuseppina Tusa[1], Tiziana Tuvè[1], Elisa Varini[2]

(1) Istituto Nazionale di Geofisica e Vulcanologia, Sezione di Catania – Osservatorio Etneo, Catania, Italy
(2) CNR – Institute for Applied Mathematics and Information Technologies Enrico Magenes, Milan, Italy

Article history: received September 12, 2024; accepted December 15, 2024

Abstract

In this study, seismic hazard, a component of the multi-hazard assessment studied in the framework of the PANACEA project, was performed following the probabilistic approach (PSHA) based on historical macroseismic data. This approach uses intensity site observations to compute the seismic history for each investigated locality. Site seismic histories completeness are improved the integrating observed intensities with "virtual" values calculated according to attenuation laws, starting from the earthquake parameters (epicentre and epicentral intensity). The probability distribution of the expected intensities at a given site is calculated for exposure times of 10, 30 and 50 years. Results are given as reference intensity and peak ground acceleration for a chosen exceeding probability. In order to obtain hazard also in terms of expected peak ground acceleration (PGA) a relation between macroseismic intensity and ground acceleration calibrated for Mt. Etna was also developed. A PGA value was predicted for each intensity site observation using a specific ground motion model for Mt. Etna shallow events, assuming a soil class A. We tested the performance of the obtained relationship through synthetic and observed PGAs associated with the most energetic seismic event instrumentally recorded at Etna. Finally, the probability distribution for PGA at the site for a given exposure time results from the combination of the corresponding seismic hazard curve for the macroseismic intensity and the specific local intensity-PGA relationship.

Keywords: Mt. Etna; Volcano-tectonic earthquakes; Seismic hazard; Macroseismic intensity; Peak ground acceleration; Earthquake scenario

1. Introduction

The INGV project "Pianeta Dinamico, Tema 8 PANACEA" (Azzaro et al., 2023; Pessina et al., 2023) promoted an integrated analysis of the different hazards affecting the volcanic region of Mt. Etna in order not to be caught unprepared and implement proactive policies of risk reduction in this highly exposed area. In this framework, the purely volcanic hazardous components of hazard – that is the eruptive phenomena such as lava flows, tephra fallout, and pyroclastic flows – were studied integrated with the seismic hazard connected to the local volcano-tectonic

seismicity. This multi-disciplinary approach, for the first time applied at Etna, is fundamental to develop impact scenarios which, not rarely, may occur simultaneously, and to carry out multi-risk analyses for territorial planning and civil protection purposes.

Among the different hazards affecting the area, only lava flows and earthquakes exhibit permanent effects heavily conditioning the territorial development. The hazard-related seismicity is not necessarily associated with the eruptive activity of Etna, since strong or even destructive earthquakes occurr during periods of "volcanic quiescence" as well. However, statistical analyses of historical data (Bevilacqua et al., 2022) demonstrated that the probability of occurrence of damaging earthquakes increases of 5-10 times after the onset or the end of flank eruptions, and this effect lasts for 30-45 days. While the destructive lava flows at a low altitude are rare (Branca et al., 2015, 2017) – eruptive fissures mostly open in the deserted areas of the upper sectors of the volcano and invade agricultural lands at a middle altitude (down to ca. 800 m asl) (Branca and Del Carlo, 2005; Del Negro et al., 2013) – the volcano-tectonic earthquakes are extremely frequent and produce heavy damage to the densely urbanized areas of Etna (D'Amico et al., 2016; Meroni et al., 2016; Pessina et al., 2021). The features of seismicity at Mt. Etna volcano are: i) moderate magnitudes ($M_L \leq 5.2$); ii) very shallow focal depths ($H < 4$ km) and iii) strong attenuation of the seismic energy (Azzaro et al., 2017; Tusa et al., 2020). As a result, the impact of this kind of events is characterized by a high spatial variability, with damage areas of limited extension located along several active faults displacing the eastern and southern flanks of the volcano.

In this paper we present the approach used for assessing seismic hazard at a local scale of Etna, and the obtained probabilistic maps that are considered for the multi-hazard and risk analysis (Garcia et al., 2024; Pessina et al., 2024). Considering the aims of the PANACEA project (Azzaro et al., 2023; Pessina et al., 2023), the seismic hazard is therefore computed without taking into account the purely tectonic regional seismicity, whose contribution in this area is important only in the long-term analyses (Azzaro et al., 2008). Finally, applications to earthquake scenarios and seismic risk assessment are also discussed.

2. Methodological approach

The probabilistic procedure adopted to assess seismic hazard at Mt. Etna is the so-called "site approach". This method is based on the use of macroseismic data, that is the dataset of the intensity values reported for a given locality defining its seismic history (Magri et al., 1994; Albarello and Mucciarelli, 2002). Although the "standard" Cornell approach has been also applied at Etna (Peruzza et al., 2017), results are strongly dependent from the assumptions and the calibration of models adopted for the computation (Azzaro et al., 2017). For this reason, we

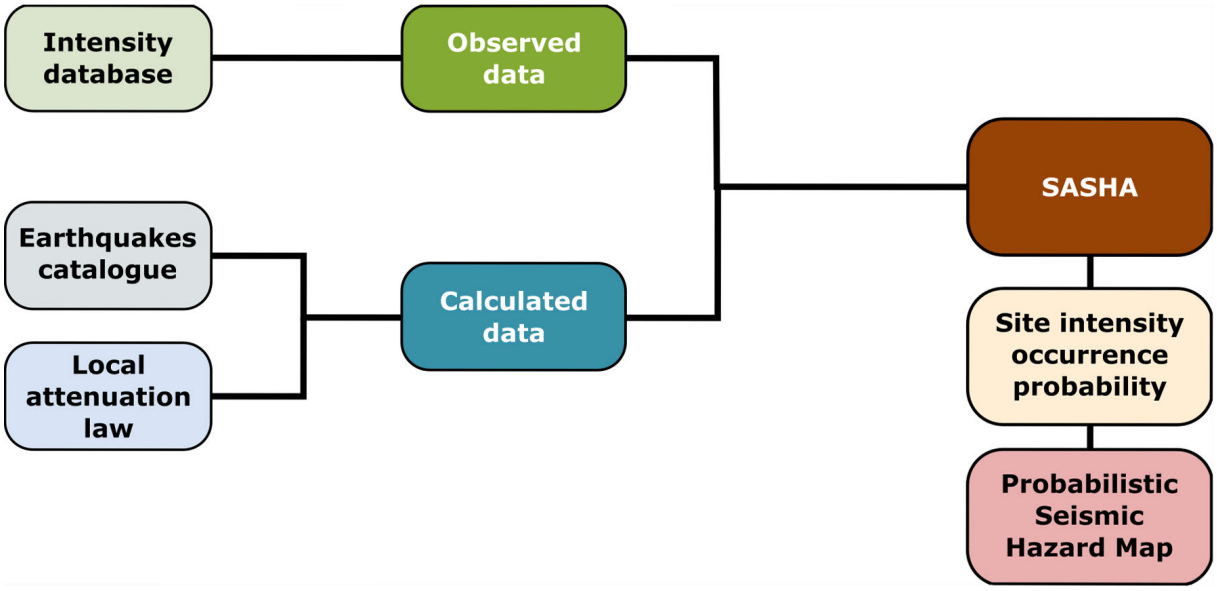

Figure 1. Flow chart illustrating the process for computing PSHA according to the "site approach" by the SASHA code (D'Amico and Albarello, 2008).

preferred this simpler procedure since it does not require any pre-processing of data such as aftershock removal to select a main shock within seismic sequences, or assumptions about seismotectonics zoning and earthquake recurrence models. The "site approach" is particularly robust when used with rich intensity datasets, as in the case of Etna, and allows using the documented effects produced by the past events over significantly long time-spans.

The software SASHA (D'Amico and Albarello, 2008) carries out the computation according to the steps (Fig. 1): (i) starting from the intensity database available for a given region (e.g. data observed at Etna), it reconstructs the site seismic histories for the localities (sites) of interest; (ii) to improve the statistical completeness of the seismic histories if a locality lacks observed data for some earthquakes, the software calculates the virtual intensity expected by means of an attenuation law, considering the epicenter and the related intensity (I_0) reported in the earthquake catalog; (iii) the software calculates the probability distribution of the expected intensity at a given site for a defined exposure time. The entire process is finally completed mapping the hazard on a grid map in order to have a continuous spatial representation.

Virtual intensities are calculated using the attenuation law specific for Etna since the relations commonly used in tectonic settings are inapplicable in volcanic regions, characterized by a high attenuation of the seismic intensity (Azzaro et al., 2006). We used an approach based on Bayesian statistics, which provides the binomial probabilistic distribution of the intensity at a given site so that it is possible to quantify the intrinsic uncertainty of the decay process (Zonno et al., 2009). The probabilistic attenuation model was adapted to the features of the Etna region (Azzaro et al., 2013) to simulate: (1) point sources (isotropic model) in which the decay is comparable to a symmetric spreading (circular), (2) linear finite sources (anisotropic model) in which the decay depends on the fault strike (elliptical, to be used when the causative fault is known). The procedure to estimate the parameters of the binomial probability distribution is reported in Rotondi et al. (2016).

3. Input data

The reference dataset for the hazard analysis is the Macroseismic Catalogue of Mt. Etna Earthquakes (CMTE, see "Data and sharing resources" section) which contains more than 1800 events, including fore- and aftershocks of low intensity. Thanks to systematic historical investigations and regular upgrades, CMTE provides a very complete picture of the historical seismicity since the 17th century. For the earthquakes above the damage threshold (epicentral intensity $I_0 \geq$ VI) in the European Macroseismic Scale (EMS, Grünthal, 1998), CMTE supplies the "Etna section" of the Parametric Catalogue of Italian Earthquakes (CPTI15, Rovida et al., 2022).

In the framework of the PANACEA project, the catalog has been improved in the time-window between 1911 and 1918, thanks to the acquisition of an historical source previously unfound (De Fiore, 1919). In particular, 55 new earthquakes were added to the catalog, and 22 were updated in the parameters. In addition, the events of the 1952 seismic sequence were revised (Azzaro et al., 2024).

For the aims of the present work, we used the whole dataset of the observed intensity contained in CMTE, whereas for obtaining the virtual intensities we considered only the earthquakes above the damage threshold ($I_0 \geq$ VI EMS); in the end, a dataset of 9070 intensity values referring to 140 events with local magnitudes M_L in the range from 2.6 to 5.2, were elaborated. As shown in Fig. 2, most of these events are located in the eastern flank of the volcano, but it is noteworthy that all the destructive events (some ten with $I_0 \geq$ VIII EMS) occurred in the area among the towns of Acireale, Giarre and Zafferana, the most populated sector of the volcano (Meroni et al., 2016). These earthquakes are due to the seismotectonic activity of the Timpe fault system (Azzaro et al., 2012).

Regarding the distribution of the observed intensity data related to these events, Fig. 3 shows that 415 localities reported in the macroseismic database (53 of which are municipalities) appear ''clustered'' in the eastern flank, where there are major settlements – the city of Catania included – characterized by exceptionally well documented seismic histories, i.e. the dataset of macroseismic observations referred to a given locality during time. Among them, the towns of Acireale and Zafferana, located at the boundary of the Timpe seismogenic zone (Fig. 2), have more than 100 observations each. Many other municipalities (36) and minor settlements (88) are also characterized by "rich" seismic histories (10-100 intensity data per site). Finally, albeit many of the localities reported in the database (65%) have a low number of macroseismic observations (<10), they mainly refer to small settlements or hamlets.

Figure 4 illustrates four situations typical for the Etna region, obtained by disaggregating the seismic histories reported in the Italian Macroseismic Database (DBMI15, see "Data and sharing resources" section) to distinguish intensity data due to local volcano-tectonic events (red circles) from those related to regional tectonic events (blue

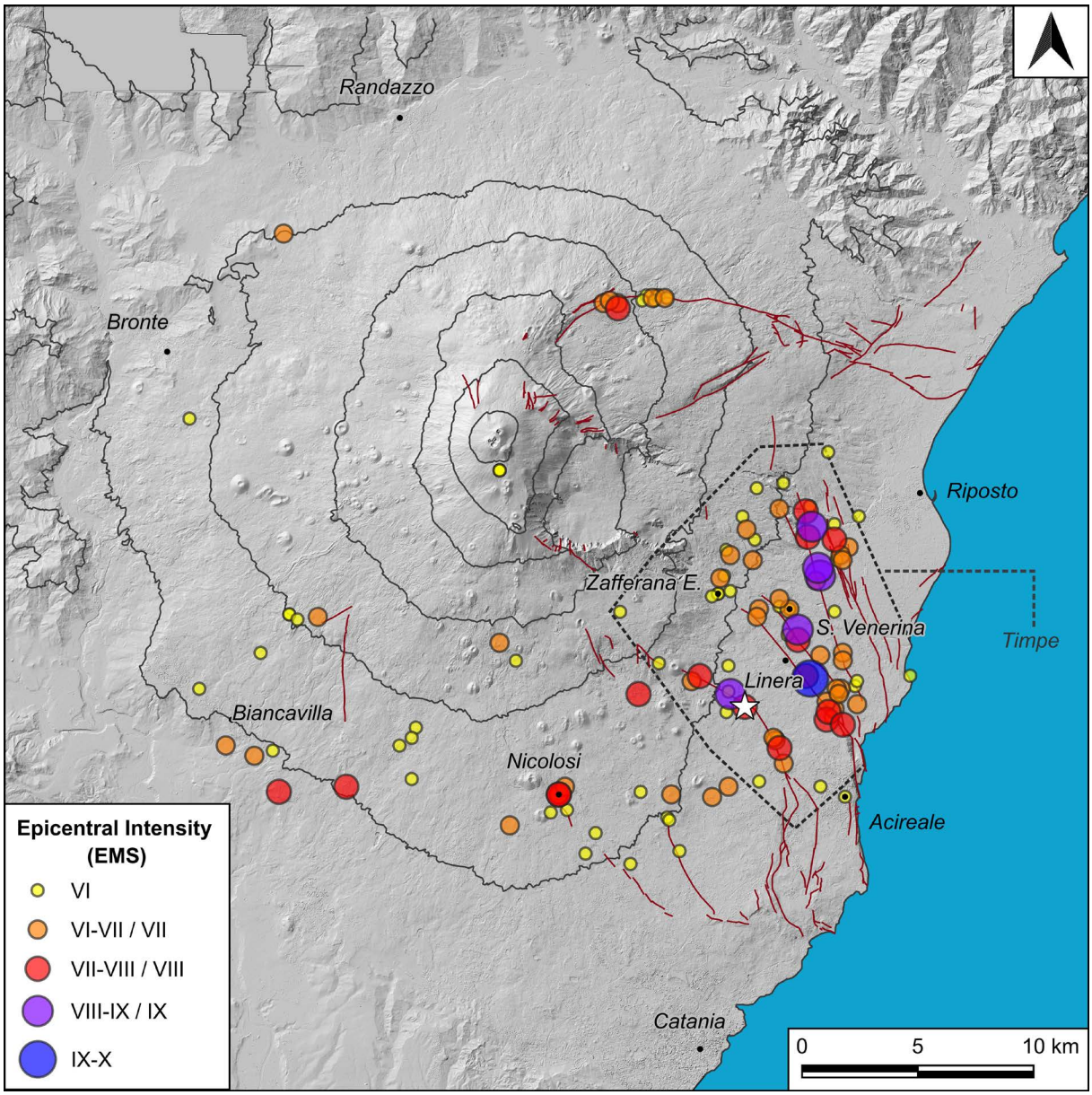

Figure 2. Location map of damaging earthquakes ($I_0 \geq$ VI EMS) occurring in the Etna area from 1600 to 2023 (data from CMTE, see "Data and sharing resources" section). Solid red lines indicate the main active faults (from Azzaro et al., 2012). The white star indicates the 2018 earthquake discussed in chapter 7.

circles): (i) localities with maximum intensities clearly due to regional events (e.g. Acireale and Catania); (ii) localities with high intensities determined both by regional and local earthquakes (e.g. Zafferana); (iii) localities characterized by maximum intensities deriving from Etna events only (e.g. S. Venerina). This kind of analysis is essential to understand the role of the volcano-tectonic earthquakes in the seismic hazard of different sectors of the volcano. It is noteworthy the case of Catania, more times severely damaged and even twice raised to the ground by regional events but never hit by Etna earthquakes (Azzaro, 1999).

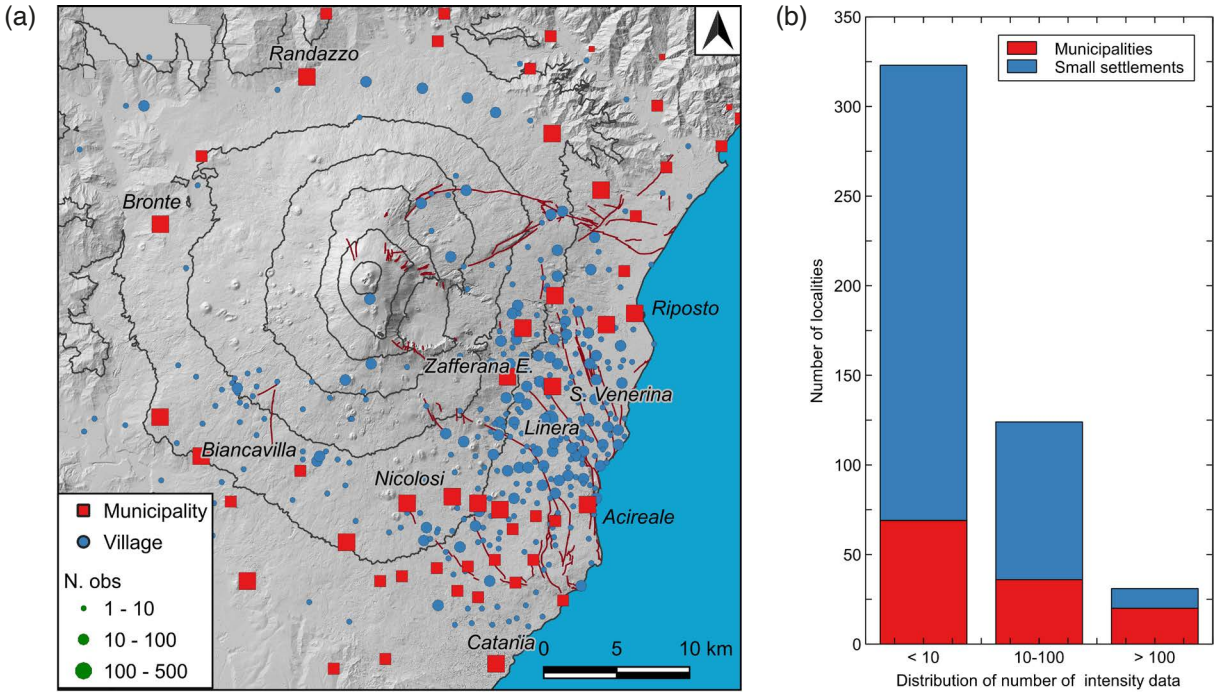

Figure 3. (a) Distribution and number of intensity data for the localities reported in the macroseismic database, considered in the hazard analysis; (b) Classification of the localities according to the relevance of the seismic histories.

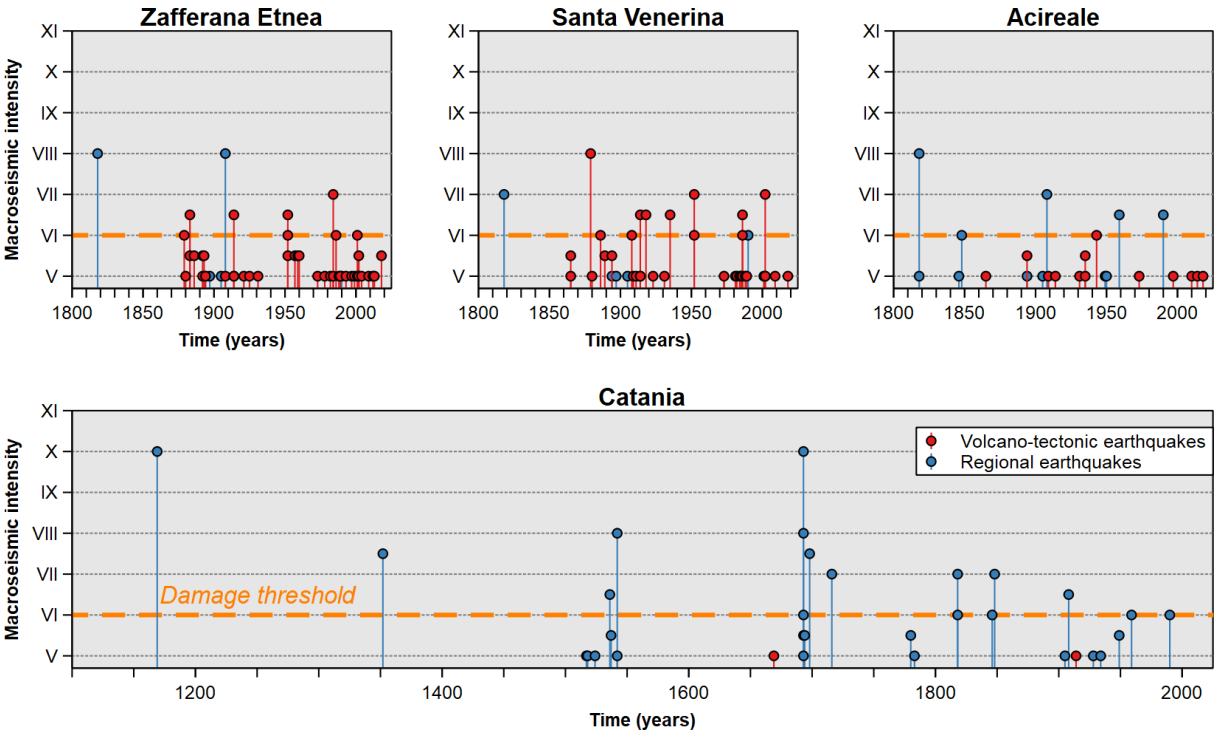

Figure 4. Examples of seismic histories determined by volcano-tectonic (red circles) and regional (blue circles) seismic sources. Data from DBMI15. Dashed orange line indicates the damage threshold (VI EMS).

4. Seismic hazard

The intensity-based PSHA procedure returns the exceedance probability for each intensity values I = 1,2,...,12, in a given exposure time. The computation takes into account the intrinsic uncertainty of macroseismic data, such as the ranges of intensity degrees such as VI-VII, VII-VIII, etc. (not meaning half-degree) etc. as well as the statistical completeness of the local seismic history data.

Figure 5 shows the hazard curves calculated for some localities of the Etna territory, considering exposure times of 10, 30 and 50 years. This representation provides the probability distribution of each expected intensity (I_{exp}), compared with the maximum intensity (I_{max}) historically observed at that site. It is noteworthy highlighting how the features of hazard change in different localities: for example, in Giarre and Zafferana the probability to suffer moderate intensities (degree VI or VII EMS, comparable with their I_{max}) is equal to 60% for an exposure time of 30 years, whereas the probability collapses to 3-5% for higher degrees. This means that the hazard is dominated by slightly damaging frequent events. Conversely, in Nicolosi and Linera the probability of having the same moderate intensities rises to 70-90% in 30 years, whereas higher intensities (comparable with their I_{max}) have probabilities in the range 10-20%. Therefore, in these localities the hazard is significantly higher, with destructive earthquakes possible (but not frequent) and moderately damaging events almost "unavoidable".

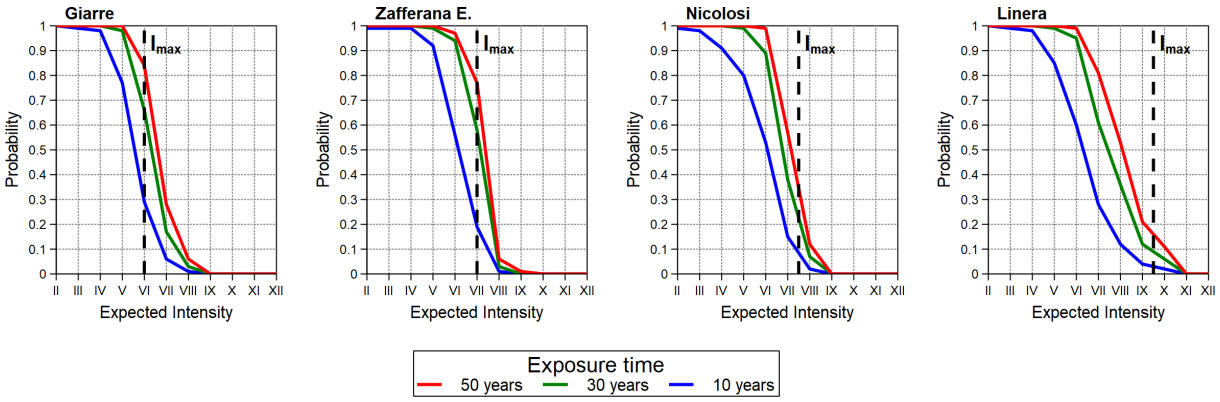

Figure 5. Examples of seismic hazard estimated at a site, considering only the volcano-tectonic seismicity. The curves show the probability distribution of the expected intensity (I_{exp}) for some localities representative of Etna, calculated for different exposure times; vertical dashed black line indicates the maximum intensity (I_{max}) historically observed at that site.

Finally, the ultimate step is representing the hazard on a map. In order to have a dense and continuous coverage of the hazard on the territory, we need to integrate the site estimations above discussed with the virtual intensities obtained from the attenuation relationships (see chapt. 2). The computation procedure is again repeated on a grid with nodes spaced 500 m. Figure 6 shows the final result of hazard, where each node represents the intensity (I_{ref}) having an exceedance probability ≥10%, calculated for a given exposure time.

It is evident that the highest values of I_{ref} are distributed in the eastern flank of the volcano, and particularly in the area crossed by the Timpe tectonic system. The map calculated for an exposure time of 10 years – interval representative of the high seismic rate at Etna – shows a maximum value of I_{ref} = VIII along these faults, whereas I_{ref} = VII affects a wide area among Zafferana, Acireale, Riposto and Nicolosi (at the northern tip of the Tremestieri fault); two spots are also present along the western segment of the Pernicana fault and at Biancavilla. The exposure time of 30 years produces a similar pattern, but the extension of I_{ref} = VIII area now embraces a wider area around the Timpe faults, and I_{ref} = VII affects almost all the volcano. Importantly, two spots of I_{ref} = IX appear along the S. Tecla and Moscarello faults. As for the rest of the Etna region, both maps are characterized by a background value of I_{ref} = VI. Finally, the hazard map obtained for an exposure time of 50 years basically confirms the pattern before observed, but we note a small area with I_{ref} = X along the S. Tecla fault – corresponding to the largest earthquake occurred at Etna (1914, M_L 5.2) – and two spots of I_{ref} = VIII at Nicolosi and Biancavilla.

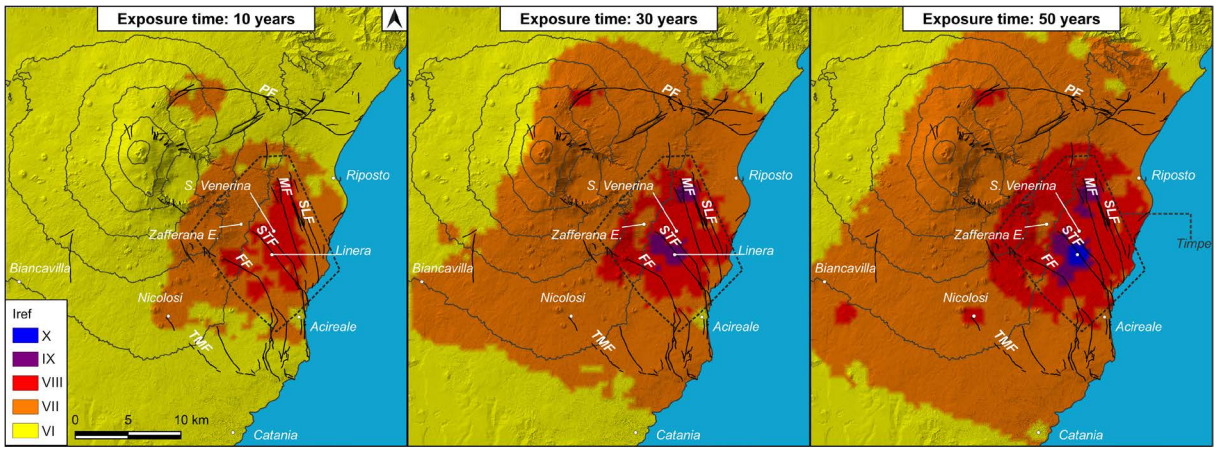

Figure 6. New seismic hazard maps expressed in terms of expected intensity (I_{ref}) with an exceedance probability of 10%, calculated for different exposure. PF: Pernicana fault; SLF: San Leonardello fault; MF: Moscarello fault; STF: Santa Tecla fault; FF: Fiandaca fault; TMF: Tremestieri fault.

5. Macroseismic intensity to peak ground acceleration conversion

The most recent models to estimate damage levels in seismic risk analyses make use of peak ground acceleration (PGA) values. In case of hazard results expressed in terms of macroseismic intensity, as in the present study, a conversion from intensity to peak ground acceleration (I-PGA) has to be applied. The concept of macroseismic intensity revolves around the idea that, for a particular place hit by an earthquake, a certain level of shaking reflects an ensemble of effects experienced in that site. Since the intensity is essentially place-related, it also "includes" the local effects of amplification and the vulnerability degree of buildings. The intensity is not a numerical value but a discrete quantity that summarizes an earthquake scenario into a degree of a macroseismic scale. While the intensity is assigned to a locality identified by convention with a geographic point, which generally represents the most historically representative point, PGA is a precise punctual measure referred to the seismic station located at a certain distance from seismic source and depending by the soil conditions.

Several formulations of I-PGA empirical relation exist in the literature for Italy (Faccioli and Cauzzi, 2006; Faenza and Michelini, 2010; Gomez-Capera et al., 2020), but they are not applicable in volcanic areas since the very different features of seismic sources and attenuation process. Taking advantage of the existence of a ground motion model specific for the Etna region (TLA20, see Tusa et al., 2020), we therefore derived a I-PGA relationship to be used for the purposes of the Panacea project.

5.1 Input data and results

In order to calibrate the conversion relationship, we selected from CMTE a dataset of 3,383 macroseismic Intensity Data Points (IDPs) spanning from degree III to IX-X EMS, related to 627 shallow earthquakes with M_L in the range 2.3-5.2. Each IDP represents a single geographic point (a locality, both municipality or minor settlement) to which a value of macroseismic intensity (I_x) is associated. Only IDPs with distance less than 30 km from the epicenter of the earthquake which produced the related effect, were considered.

For each IDP we calculated the PGA value by using the TLA20-60b (recordings with epicentral distances lesser than 60 km). Predicted PGA values were calculated for the 627 selected earthquakes, given M_L and distance between the epicentre and the considered IDP, for soils of "class A". When no instrumental magnitude was available, as for the historical pre-instrumental earthquakes, macroseismic magnitude and epicenter reported in CMTE were used.

To perform the regression through the least-squares method between observed intensity I_x and the logarithm of calculated PGA, some constraints have to be given. We assumed I_x as an independent variable, being intensity a discrete quantity that represents a sort of bin containing several $\log_{10}$(PGA) values, not uniformly distributed in each I_x bin. Since an uncertainty between all the PGA values obtained for the same macroseismic degree is expected, a mean value for each bin has been calculated and then fitted by the least-squares method (Fig. 7a).

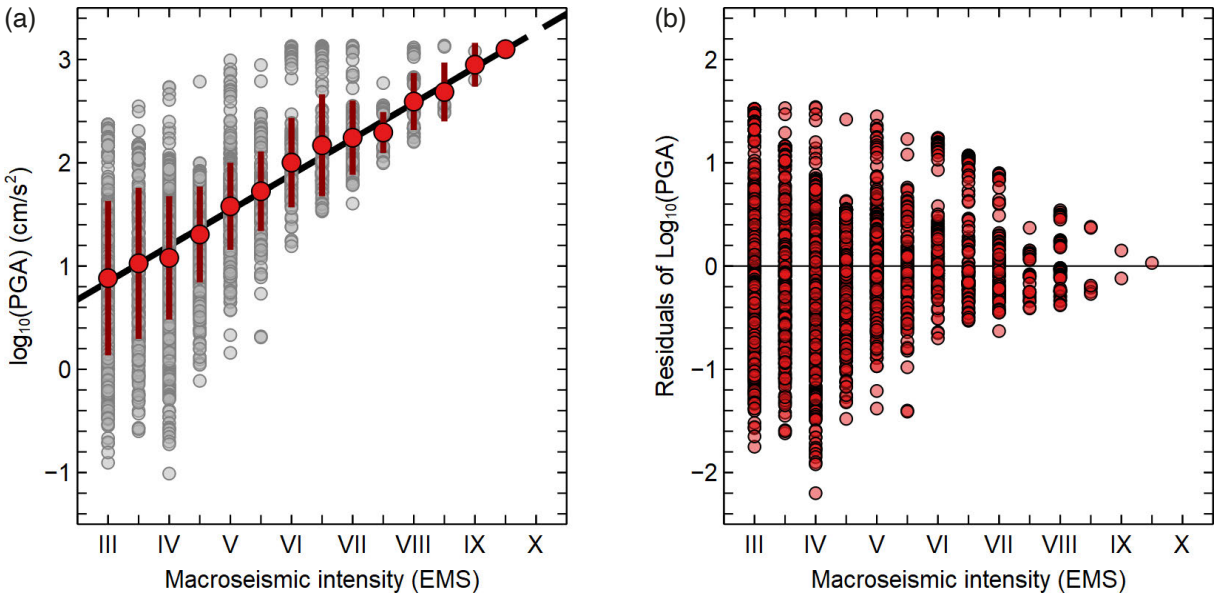

Figure 7. (a) Linear regression of the observed macroseismic intensity vs peak ground acceleration (PGA) calculated by the Tusa et al. (2020) ground motion model. (b) Analysis of the residuals between observed and calculated PGA vs macroseismic intensity.

The final relation is:

$$\log_{10}(\mathrm{PGA}) = 0.346(\pm 0.01) \cdot I_x - 0.190(\pm 0.063) \tag{1}$$

with determination coefficient $R^2 = 0.991$, standard error $S_E = 0.073$ and Pearson correlation coefficient $\rho = 0.995$.

The analysis of residuals (Fig. 7b) – differences between the observed and predicted values in a regression model – provides indication on the accuracy of the prediction: the plot of the residuals versus observed macroseismic intensity shows a somewhat random pattern with mean $\mu = -0.026$, indicating that the model provides a reliable fit to the data with an overall variance of $\sigma^2 = 0.345$. In detail, variance is decreasing from intensity III to IX, so that a value for each intensity class, was calculated. Residuals for intensity degrees with uncertainty (as VI-VII) were grouped to the lower intensity bin. Variance $\sigma^2_{I_X}$ of each intensity bin is: $\sigma^2_3 = 0.547$, $\sigma^2_4 = 0.322$, $\sigma^2_5 = 0.168$, $\sigma^2_6 = 0.209$, $\sigma^2_7 = 0.106$, $\sigma^2_8 = 0.073$, $\sigma^2_9 = 0.019$.

5.2 Probabilistic prediction of PGA and final maps

For a given value of intensity I_x at site, the I-PGA relationship (Eq. 1) calibrated for Mt. Etna describes the base 10 logarithm of the PGA_x at site as a Gaussian random variable with mean (0.346 I_x – 0.190) and standard deviation taken from the square root of variance of the residuals of Fig. 7b, because $S_E = 0.073$ is the error of the average fit and does not represents the real dispersion of the data:

$$\log_{10}(PGA_x)|I_x \sim \Phi\left(\frac{\log_{10}(PGA_x) - (0.346 I_x - 0.190)}{\sigma_{Ix}}\right), \tag{2}$$

where Φ denotes the standard Gaussian distribution and σ_{Ix} is the square root of the variance calculated for each intensity I_x.

As suggested by D'Amico and Albarello (2008), this allow to compute PGA-based PSHA via the intensity-based PSHA obtained from the SASHA software, which provides the probability distribution of the intensity at a given site, i.e. $Prob(I_x = i)$ for all $i = 1,2, \ldots, I_{max}$, with $I_{max} = 12$, the maximum degree of the macroseismic scale.

Since there is a chance that PGA_x exceeds a given pga value for each value of I_x according to Eq. (2), the exceedance probability $Prob(PGA_x \geq pga)$ is calculated via the law of total probability:

$$Prob(PGA_x \geq pga) = 1 - \sum_{i=1}^{I_{max}} Prob(I_x = i) \cdot \Phi\left(\frac{\log_{10}(pga) - (0.346 \cdot i - 0.190)}{\sigma_{Ix}}\right) \quad (3)$$

The result is the PSHA expressed in PGA for site x, with exposure time equal to that of the intensity-based PSHA. Since the PGA is a real value, we computed Eq. (3) on a discrete set $\{pga_k: k = 0, 1, \dots, K\}$ of PGA values. To reduce the computational effort in evaluating Eq. (3) for a large number $\mathcal{S}$ of sites, we organized all quantities in matrix form:

$$\mathrm{H} = \mathrm{U} - \mathrm{PF} \quad (4)$$

where P is the $\mathcal{S} \times I_{max}$ matrix with elements $Prob(I_x = i)$, F is the $I_{max} \times (K+1)$ matrix with elements $Prob(PGA_x < pga_k | I_x)$ given by Eq. (2), and U is the $\mathcal{S} \times (K+1)$ matrix with all elements equal to 1. Based on Eq. (4), one can obtain approximations of the probability density function as well as other proxies regarding the probability distribution Eq. (3).

6. Strong ground-motion simulations

Synthetic simulations represent a powerful method for validating the relationships among different ground motion parameters – typically peak ground acceleration (PGA), peak ground velocity (PGV) and macroseismic intensity – and testing their performance mostly for the rare and strongest seismic events. To be realistic, they require a comprehensive approach that integrates source modeling, wave propagation, local site effects, and stochastic variability of motion. In this work, we applied the code EXSIM (Extended fault SIMulation) by Motazedian and Atkinson (2005) for the finite-fault modeling of the strong ground motion caused by the 26 December 2018 (02:19 UTC) M_W 4.9 earthquake, the strongest event of the last 70 years at Etna. It represents the best case study for synthetic simulations, for several reasons: i) it is the shallow strongest earthquake ever instrumentally recorded at Etna; ii) it represents the typical volcanic-tectonic event capable of causing heavy damage; iii) it has been extensively studied, so the literature provides numerous constraints for realistic numerical simulations (e.g., De Novellis et al., 2019; Azzaro et al., 2022).

6.1 Input data and model parameters

The strong ground motion data were acquired by the accelerometric stations of the Italian National Seismic Network (RSN – INGV) and the Italian National Accelerometric Network (RAN, operated by the Civil Protection Department). The highest PGA values, 0.56 g and 0.30 g, were recorded respectively at the stations SVN and EVRN, the closest ones to the epicenter at a distance of 5 km.

As for the input parameters, we need to constrain a complete finite-fault model (including geometric-kinematic and source parameters), and to consider the crustal properties of the region (controlling the geometrical spreading coefficient and the anelastic attenuation) as well as the local site effects.

6.1.1 Seismic source and propagation path parameters

The 26 December 2018 earthquake is related to the Fiandaca fault (FF), the westernmost structure of the Timpe tectonic system in the volcano's eastern flank (see Fig. 1 and Fig. 6). Together with the 1894 earthquake, this event entirely ruptured the FF for a length of ca. 7.5 km (Azzaro et al., 2022). From the moment tensor inversion, the best solution proposed for the focal mechanism indicates a mainly right-lateral kinematics (rake –158°) along a NW-SE trending vertical plane (strike N306°E and dip 88° dip towards NE) (https://terremoti.ingv.it/). The 3D-geometry

of FF has been derived by Cannavò et al. (2016), who estimated a length of 7 km and a width of 2.6 km through the inversion of ground deformation data. The fault has been then discretized by 28 sub-faults of 1000×650 m^2 each, whilst the top of the fault intercepts the surface, as indicated by the impressive co-seismic surface faulting produced by the earthquake.

Table 1 summarizes the parameters required for the stochastic finite-fault simulations, and their final values established on the base of the misfit function between observed and synthetic PGAs (see Eq. 5). The M_W from 4.8 and 5.0 includes the range of values reported by the seismological literature for this event. The stress parameter $\Delta\sigma$ represents a decisive element for numerical simulation, since it corresponds to the energy concentration along the fault and controls the high frequency content of the simulated acceleration time series. The range of stress drop parameter used for simulations has been derived from Saraò et al. (2023) for shallow events at Etna (focal depth less than 5 km) and M_L higher than 4.0. Note that the same authors estimated a stress drop of 2.9 MPa for this earthquake.

Parameter	Values	Reference
Magnitude M_W	4.8-5.0 (final value 4.9)	
Stress drop, $\Delta\sigma$	1-3 MPa (final value 2.5 MPa)	Saraò et al., 2023
Density at the source, ρ	1800 kg/m^3	Christensen and Mooney, 1995
Shear wave velocity at the source, Vs	1.8 km/s	Langer et al., 2016
Rupture velocity	0.8/Vs	
Length of fault	7 km	Cannavò et al., 2016
Width of fault	2.6 km	Cannavò et al., 2016
Depth of the top of the fault plane	0 km	
Fault orientation (strike & dip)	306-88	
Pulsing area	50-80% (final value 50%)	
Rise Time	$1/f_0$, where f_0 is the source corner frequency	
Geometrical spreading	$g(R) = R^{-1}$ per $R \leq R_1 = 40$ km	Scognamiglio et al., 2005
	$g(R) = [(1/R_1) \times (R_1/R)^{-0.4}]$ per $R > R_1$	
Anelastic Attenuation	$Q(f) = 45\ f^{0.77}$	Giampiccolo et al., 2024
f_{max}	5-15 Hz (final value 15 Hz)	Langer et al., 2016
Slip distribution	Random	
Windowing function		Saragoni and Hurt, 1974

Parameter	Values	Reference
Distance-dependent duration	this study	
Crustal model for Etna		Hirn et al., 1991

Table 1. Model parameters used in finite-fault simulations of the 26 December 2018 earthquake.

Path effects, due to both attenuation characteristics of the rock media through which the waves propagate from the source to recording site, and shallow subsurface geology, represent an important component in ground motion modeling surface. Besides we need to specify the geometrical spreading and total path duration effects. The anelastic attenuation is given by the frequency-dependent quality factor found recently by Giampiccolo et al. (2024) for the shallow crust at Mount Etna, that is $Q(f) = 45\ f^{0.77}$. According to Langer et al. (2016), we use two regimes for the geometrical spreading: R^{-1} for distances less than 40 km, and $R^{-0.4}$ for larger distances (Scognamiglio et al., 2005).

The crustal amplification (Atkinson and Boore, 2006), which describes the combined effects of the velocity gradient with depth and the impedance structure of the shallow layers, has been taken into account defining a frequency-dependent amplification function calculated using the propagator-matrix method of Haskell (1960). This function was specified considering the 1D-shear wave velocity for Etna by Hirn et al. (1991), and assigning to each layers the density values (ρ) derived by using the empirical relations from Christensen and Mooney (1995) (through the P-wave velocities).

6.1.2 Distance-dependent duration model

To fully account for the path effects, the path-dependent duration model (TP) has to be considered. Often the relation TP = 0.05R (where R is the source-to-site distance in km) by Hermann (1985) is used (see Fig. 8). Within the scope of stochastic simulations, Boore and Thompson (2014) referred to significant duration determined from the Husid plot (Husid, 1969) and based on the interval T during which a certain portion of the total Arias intensity is accumulated (e.g., 90%, defining the parameter T90 considered in this study).

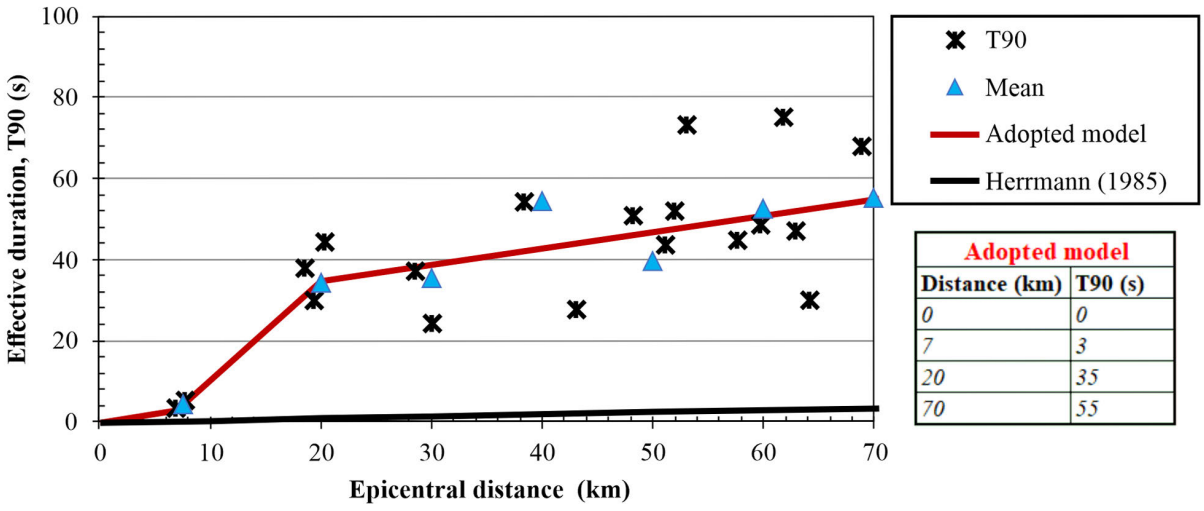

Figure 8. T90 vs epicentral distance for the 26 December 2018 earthquake recorded by the accelerometric stations within 70 km from the epicenter used to derive the path duration model for the synthetic simulations (asterisks). T90 values are from the ITalian ACcelerometric Archive (ITACA, see "Data and sharing resources" section). The path duration models by Herrmann (1985) is reported, as well, for comparison purposes. The white blue triangles indicate the mean values used for linear regression analysis (see text for details). The inset in the bottom left corner, explicitly depicts the final path duration model adopted for numerical simulations.

In our case, the contribution of source duration on T90 can be considered negligible, since it is about 0.5s (= $1/f_0$, where f_0 is the corner frequency in Hz), as suggested by the value of $f_0 = 2.0$ Hz estimated by Saraò et al. (2023) for the 26 December earthquake. Therefore, we can pose TP ≅ T90. We have computed the values of T90 for this earthquake from the strong motion stations within 70 km from its epicentre (Fig. 8) Then, we derived the final path duration model taking into account the mean values of T90 in distance bins of 10 km (light blue triangles in Fig. 8), dividing them in three different series, and estimating the regression lines through the data from each single series (1 to 3 in Fig. 8). Note, however, that the first series contains the T90 values for the first 7 km.

6.2 Simulation results

We carried out simulations varying the key input parameters in EXSIM in order to match as best as possible the observed PGAs and PGVs. Although not directly involved in the estimation of I-PGA empirical relation in this study, we also considered PGV since it provides further constraints. In fact, PGA and PGV offer complementary information about ground motion at higher and lower frequencies, respectively.

For each combination of input parameters, we computed a misfit function between the observed and synthetic PGMs as follows (Convertito and Pino, 2014):

$$f(x) = \frac{\sum_{i=1}^{N}(PGMobs - PGMsyn)^2}{\left(\sum_{i=1}^{N} PGMobs\right)^2} \tag{5}$$

where N is the total number of observations (in our case N = 14). The best set of input parameters was the one that minimized f(x) for both PGA and PGV at the same time.

As shown in Table 1, the best results are obtained for $\Delta\sigma = 2.5$ MPa, $M_W = 4.9$, and pulsing percentage = 50%. Regarding the high-frequency spectral roll-off of ground acceleration, EXSIM allows to model it by either the two high-cut filters, f_{max} (Hanks, 1982) and kappa (κ) (Anderson and Hough, 1984), which can be used interchangeable. Here, we adopted the f_{max} filter, varying its value from 5 to 15 Hz. As reported in Table 1, we obtain the best match with the observations for f_{max} equal to 15 Hz.

Figure 9 shows the comparison between recorded and synthetic PGMs. On average, the synthetic data seem to describe the observed PGAs and PGVs well, although we did not explicitly account for site effects. However,

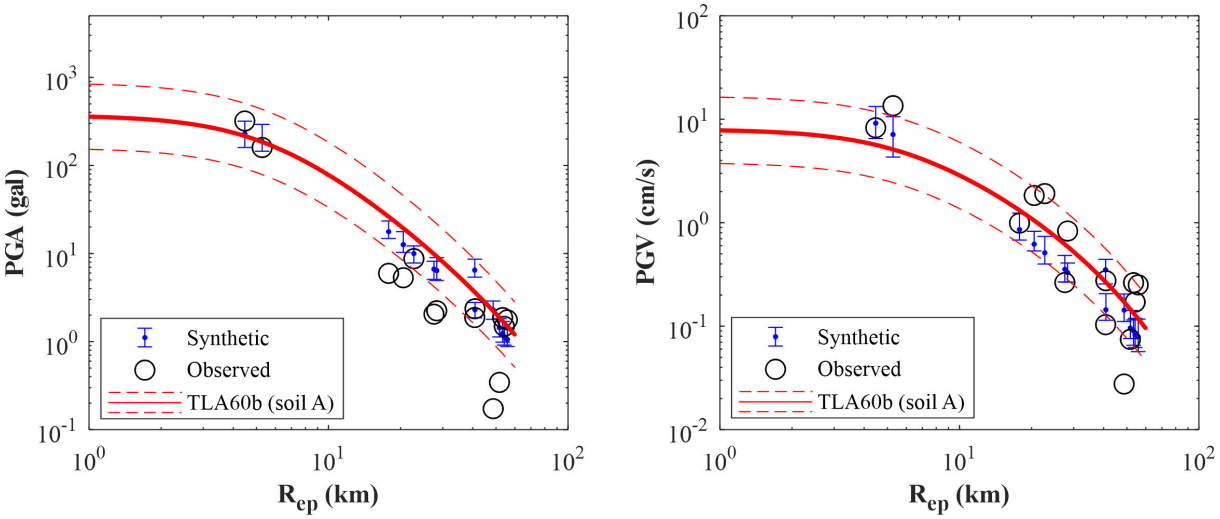

Figure 9. Comparison between synthetic (blue dots) and observed (circles) PGAs and PGVs for the 26 December 2018 earthquake. In each panel the predicted PGMs by the GMMs proposed by Tusa et al. (2020) (TLA60b) for a $M_W = 4.9$ are shown (red lines). The continuous red lines correspond to the mean values of the GMM, the dashed red lines correspond to ±σ, and the vertical bars correspond to the minimum and maximum values of PGMs obtained from each realization with EXSIM.

most of the strong motion stations are installed on soil classes A and B (9 and 3, respectively, out of a total of 14), suggesting that they are supposed not be affected by strong site effects. We additionally compared the synthetic PGMs with predicted by the GMM TLA60b (Tusa et al., 2020), specifically calibrated for the shallow seismic events at Mount Etna. In Fig. 9, the ground motions simulated for the 26 December 2018 earthquake follow trends that closely overlap with that predicted by the GMM.

The simulated PGMs are well within the uncertainty range, suggesting the reliability of the adopted parametrization. Therefore, the associated set of input parameters give us a meaningful way to reproduce the ground-motion shaking at the localities for which the macroseismic intensity is the only available source of information, including the sites in the epicentral area suffering the heaviest damage. Figure 10 shows the comparison between the synthetic and predicted PGAs as a function of Joyner-Boore distance (R_{jb}) (i.e. the minimum distance from the surface fault projection) for the 43 localities classified in terms of macroseismic intensity. The simulated ground motions follow trends that closely overlap with that predicted by the GMM TLA60b for M_W 4.9. The synthetic PGAs range from ca 0.01g at $R_{jb} = 20$ km to 1g at $R_{jb} = 0.1$ km from the fault. In Fig. 11, it is evident that the I-PGA relationship described by Eq. (1) tends to underestimate the PGA values for this event. In fact, for a grade VIII of macroseismic intensity, the I-PGA relationship estimates a PGA value of approximately 0.4g compared to an average of 0.8g calculated through numerical simulations for those locations with the same intensity degree. At the same time, however, a value of 0.8g is obtained through the I-PGA relationship if intensity IX is considered. Moreover, in Fig. 11 the synthetic PGAs still overlap with the cloud of points that straddles and lies above the line representing the I-PGA relationship, suggesting that the synthetic simulations are however able to reproduce realistic PGMs, comparable with the ones attributed to other historical events that struck the volcanic area.

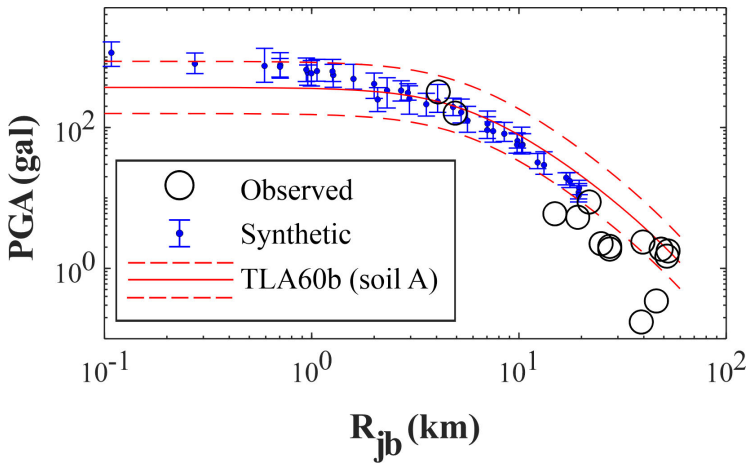

Figure 10. Comparison between synthetic (blue dots) and predicted PGAs by the GMMs proposed by Tusa et al. (2020) (TLA60b) considering a soil class A (red lines) for the 43 localities having an estimate of macroseismic intensity. The observed PGAs are shown for comparison purpose (black circles). Vertical bars correspond to the minimum and maximum values of PGAs through the numerical simulations.

7. Conclusions

In this paper, we present seismic hazard of the Mt. Etna as a component of the multi-hazard assessment which characterizes this highly exposed volcanic area. Not only the purely volcanic phenomena but also the volcanic-tectonic earthquakes are precisely documented since 1600, feature not common in other volcanic areas worldwide. Using the large updated macroseismic catalog and attenuation model specifically derived for this area (Azzaro et al., 2013), we applied the "site approach" based on intensity data (SASHA code, see D'Amico and Albarello, 2008) to obtain a zoneless PSHA. Seismic hazard maps calculated for a 10% exceedance probability and exposure times ranging from 50 to 10 years show high values of expected intensity (I_{exp}), up to degrees X, in the eastern flank of the volcano. These results confirm and improve the maps obtained in previous studies by the same methodology (Azzaro et al., 2008, 2013).

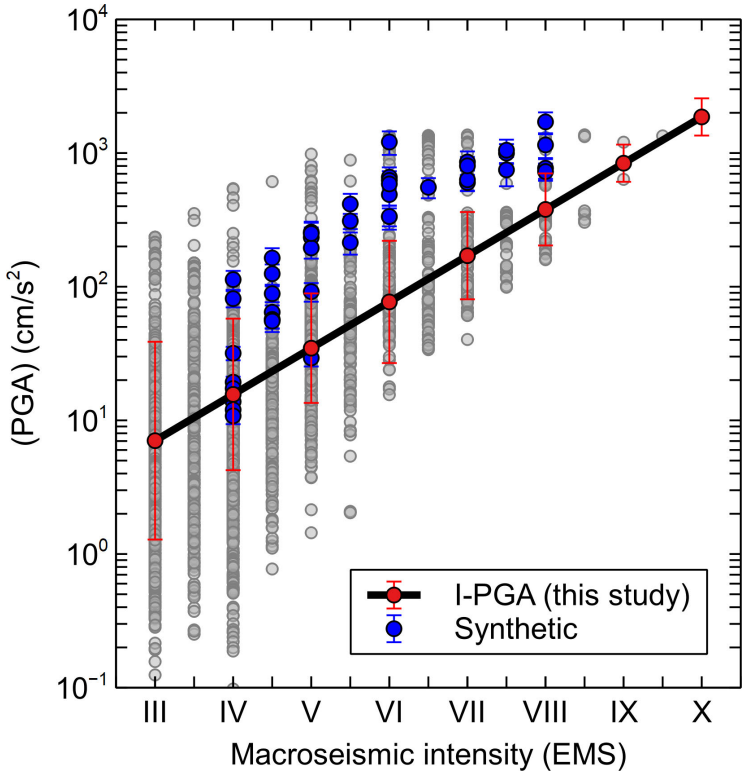

Figure 11. The same as Fig. 7a but with the overlay of synthetic PGAs for the 26 December 2018 earthquake vs macroseismic intensity. Vertical bars in synthetic PGAs correspond to minimum and maximum values, and to standard deviation σ_{Ix} of I-PGA relationship.

In order to the damage levels for seismic risk analyses (Pessina et al., 2024), a conversion relationship from intensity to peak ground acceleration (I-PGA) has been also derived and validated through the synthetic simulation of the 2018 earthquake ground motion parameters. The comparison suggests that they could be combined with real earthquake data to refine the relationship and improve predictive accuracy. At the same time, the synthetic PGAs are generally higher than those predicted by the I-PGA relationship. This result does not necessarily indicate inadequate predictive capability of the I-PGA relationship, which is intended to predict range of PGA expected for a given intensity degree.

Finally, hazard maps calculated for a 10% of exceedance probability show, for the exposure time of 30 years, PGA values ranging from 576 to 830 cm/s^2 in areas where I_{ref} = IX (destructive effects) are expected, and from 261 to 368 cm/s^2 in areas where I_{ref} = VIII (heavily damaging) are expected.

Data and sharing resources. Data used in this study were obtained from the following online resources:

- CMTE: Azzaro, R. and S. D'Amico (2014). Catalogo Macrosismico dei Terremoti Etnei (CMTE), 1633-2023 [Data set], Istituto Nazionale di Geofisica e Vulcanologia (INGV), doi:10.13127/cmte, https://www.ct.ingv.it/macro/etna.
- CPTI15: Rovida, A., M. Locati, R. Camassi, B. Lolli, P. Gasperini and A. Antonucci (2022). Italian Parametric Earthquake Catalogue (CPTI15), version 4.0 [Data set], Istituto Nazionale di Geofisica e Vulcanologia (INGV), doi:10.13127/cpti/cpti15.4, https://emidius.mi.ingv.it/CPTI15-DBMI15/index_en.htm.
- DBMI15: Locati, M., R. Camassi, A. Rovida, E. Ercolani, F. Bernardini, V. Castelli, C. H. Caracciolo, A. Tertulliani, A. Rossi, R. Azzaro, S. D'Amico, A. Antonucci (2022). Italian Macroseismic Database (DBMI15), version 4.0 [Data set]. Istituto Nazionale di Geofisica e Vulcanologia (INGV), doi:10.13127/dbmi/dbmi15.4, https://emidius.mi.ingv.it/CPTI15-DBMI15/index_en.htm.
- ITACA: Felicetta, C., E. Russo, M. D'Amico, S. Sgobba, G. Lanzano, C. Mascandola, F. Pacor, L. Luzi (2023). Italian Accelerometric Archive v4.0, Istituto Nazionale di Geofisica e Vulcanologia, Dipartimento della Protezione Civile Nazionale, doi:10.13127/itaca.4.0, https://itaca.mi.ingv.it/ItacaNet_40.

Acknowledgements. The authors wish to thank two anonymous referees for their careful review and useful suggestions that improved the original paper.
This work was supported by the INGV project Pianeta Dinamico (CUP D53J19000170001) funded by MIUR ("Fondo finalizzato al rilancio degli investimenti delle amministrazioni centrali dello Stato e allo sviluppo del Paese," legge 145/2018), Tema 8-PANACEA.

References

Albarello, D. and M. Mucciarelli (2002). Seismic hazard estimates using ill-defined macroseismic data at site, Pure Appl. Geophys., 159, 1289-1304, doi:10.1007/s00024-002-8682-2.

Anderson, J. G. and S. R. Hough (1984). A model for the shape of the Fourier amplitude spectrum of acceleration at high frequencies, B. Seismol. Soc. Am., 74, 5, 1969-1993, doi:10.1785/BSSA0740051969.

Atkinson, G. M. and D. M. Boore (2006). Earthquake ground-motion prediction equations for eastern North America, B. Seismol. Soc. Am., 96, 2181-2205, doi:10.1785/0120050245.

Azzaro, R. (1999). Earthquake surface faulting at Mount Etna volcano (Sicily) and implications for active tectonics, J. Geodyn., 28, 193-213, doi:10.1016/S0264-3707(98)00037-4.

Azzaro, R., M. S. Barbano, S. D'Amico and T. Tuvè (2006). The attenuation of seismic intensity in the Etna region and comparison with other Italian volcanic districts, Ann. Geophys., 49, 4/5, 1003-1020, doi:10.4401/ag-3113.

Azzaro, R., G. Barberi, S. D'Amico, B. Pace et al. (2017). When probabilistic seismic hazard climbs volcanoes: the Mt. Etna case, Italy – Part 1: Model components for sources parameterization, Nat. Hazard Earth Sys., 17, 1981-1998, doi:10.5194/nhess-17-1981-2017.

Azzaro, R., M. S. Barbano, S. D'Amico, T. Tuvè et al. (2008). First studies of probabilistic seismic hazard assessment in the volcanic region of Mt. Etna (Southern Italy) by means of macroseismic intensities, Boll. Geofis. Teor. Appl., 49, 1, 77-91.

Azzaro, R., S. Branca, K. Gwinner and M. Coltelli (2012). The volcano-tectonic map of Etna volcano, 1:100.000 scale: an integrated approach based on a morphotectonic analysis from high-resolution DEM constrained by geologic, active faulting and seismotectonic data, Ital. J. Geosci., 131, 1, 153-170, doi:10.3301/IJG.2011.29.

Azzaro, R., S. D'Amico, T. Esposti Ongaro, G. Ganci et al. (2023). Towards a Multi-Hazard Assessment at Etna Volcano (Italy): The PANACEA Project, in Advances in Natural Hazards and Volcanic Risks: Shaping a Sustainable Future A. Malheiro, F. Fernandes and H. I. Chaminé (Editors), Springer Nature Switzerland, Cham, Advances in Science, Technology & Innovation, 31-35, doi:10.1007/978-3-031-25042-2_6.

Azzaro, R., S. D'Amico, R. Rotondi, T. Tuvè et al. (2013). Forecasting seismic scenarios on Etna volcano (Italy) through probabilistic intensity attenuation models: A Bayesian approach, J. Volcanol. Geotherm. Res., 251, 149-157, doi:10.1016/j.jvolgeores.2012.07.011.

Azzaro, R., S. Pucci, F. Villani, R. Civico et al. (2022). Surface faulting of the 26 December 2018, Mw5 Mt. Etna earthquake (Italy): geological source model and implications for the seismic potential of the Fiandaca fault, Tectonics, 41, doi:10.1029/2021TC007182.

Azzaro, R., M. S. Barbano, D. Musumeci and G. Orefice (2024). A reappraisal of the March 1952 Linera seismic sequence: the case study of the S. Tecla fault (Mt. Etna), 42° Convegno Nazionale GNGTS, 13-16 February, Ferrara (Italy).

Bevilacqua, A., R. Azzaro, S. Branca, S. D'Amico et al. (2022). Quantifying the statistical relationships between flank eruptions and major earthquakes at Mt. Etna volcano (Italy), J. Volcanol. Geotherm. Res., Solid Earth, 127, doi:10.1029/2022JB024145.

Boore, D. M. and E. M. Thompson (2014). Path durations for use in the stochastic-method simulation of ground motions, Bull. Seismol. Soc. Am., 104, 2541-2552, doi:10.1785/0120140058.

Branca, S., R. Azzaro, E. De Beni, D. Chester et al. (2015). Impacts of the 1669 eruption and the 1693 earthquakes on the Etna Region, (Eastern Sicily, Italy): an example of recovery and response of a small area to extreme events, J. Volcanol. Geotherm. Res., 303, 25-40, doi:10.1016/j.jvolgeores.2015.07.020.

Branca, S., E. De Beni, D. Chester, A. Duncan et al. (2017). The 1928 eruption of Mount Etna (Italy) and the destruction and recovery of the town of Mascali, J. Volcanol. Geotherm. Res., 335, 54-70, doi:10.1016/j.jvolgeores.2017.02.002.

Branca, S. and P. Del Carlo (2005). Types of eruptions of Etna volcano AD 1670-2003: implications for short-term eruptive behavior, Bull. Volcanol., 67, 732-742, doi:10.1007/s00445-005-0412-z.

Cannavò, F., S. Gambino, B. Puglisi and R. Velardita (2016). Modeling ground deformation associated with the destructive earthquakes occurring on Mt. Etna's southeastern flank in 1984, Nat. Hazards Earth Sys. Sci., 16, 2443-2453, doi:10.5194/nhess-16-2443-2016.

Christensen, N. I. and W. D. Mooney (1995). Seismic Velocity Structure and Composition of the Continental Crust: A Global View, J. Volcanol. Geotherm. Res. Solid Earth, 100, 9761-9788, doi:10.1029/95JB00259.

Convertito, V. and N. A. Pino (2014). Discriminating among distinct source models of the 1908 Messina Straits earthquake by modelling intensity data through full wavefield seismograms, Geophys. J. Int., 198, 1, 164-173, doi:10.1093/gji/ggu128.

D'Amico, S., F. Meroni, M. L. Sousa and G. Zonno (2016). Building vulnerability and seismic risk analysis in the urban area of Mt. Etna volcano (Italy), Bull. Earthq. Eng., 14, 7, 1797-1811, doi:10.1007/s10518-015-9804-4.

D'Amico, V. and D. Albarello (2008). SASHA: a computer program to assess seismic hazard from intensity data, Seismol. Res. Lett., 79, 5, 663-671, doi:10.1785/gssrl.79.5.663.

De Fiore, O. (1919). Il periodo di riposo 1911-1918. L'Etna, Scuola Tipografica Sacro Cuore, Barriera del Bosco, 119.

De Novellis, V., S. Atzori, C. De Luca, M. Manzo et al. (2019). DInSAR analysis and analytical modelling of Mt. Etna displacements: the December 2018 volcano-tectonic crisis, Geophys. Res. Lett., 46, 5817-5827, doi:10.1029/2019GL082467.

Del Negro, C., A. Cappello, M. Neri, G. Bilotta et al. (2013). Lava flow hazards at Mount Etna: constraints imposed by eruptive history and numerical simulations, Sci. Rep., 3, 3493, doi:10.1038/srep03493.

Faenza, L. and A. Michelini (2010). Regression analysis of MCS intensity and ground motion parameters in Italy and its application in ShakeMap, Geophys. J. Int., 180, 3, 1138-1152, doi:10.1111/j.1365-246X.2009.04467.x.

Faccioli, E. and C. Cauzzi (2006). Macroseismic intensities for seismic scenarios estimated from instrumentally based correlations, Proceedings First European Conference on Earthquake Engineering and Seismology, 569, 3-8 September 2006, Geneva (Switzerland), doi:10.13140/RG.2.1.3984.2641.

Garcia, A., L. Sandri, V. Pessina, F. Meroni et al. (2025). A target-based, multi-hazard assessment approach as a tool for supporting decision-making in volcanic areas: a case study in Mt. Etna, Italy, Ann. Geophys., 68, 1, doi:10.4401/ag-9173.

Giampiccolo, E., T. Tuvè, F. Bianco and E. Del Pezzo (2024). Depth and Spatial Variation of the Shear Wave Attenuation Parameters in the Shallow Crust and Lower Crust/Upper Mantle of Mt. Etna (Italy), Pure Appl. Geophys., 181, 171-187, doi:10.1007/s00024-023-03400-0.

Gomez-Capera, A. A., M. D'Amico, G. Lanzano, M. Locati et al. (2020). Relationships between ground motion parameters and macroseismic intensity for Italy, Bull. Earthq. Eng., 18, 11, 5143-5164, doi:10.1007/s10518-020-00905-0.

Grünthal, G. (1998). European Macroseismic Scale 1998 (EMS-98), European Seismological Commission, Subcommission on Engineering Seismology, Working Group Macroseismic Scale, Luxembourg, 15, 1-99.

Hanks, T. C. (1982). Fmax, Bull. Seismol. Soc. Am., 72, 1867-1879, doi:10.1785/BSSA07206A1867.

Haskell, N. A. (1960). Crustal reflection of plane SH waves, J. Geophys. Rese., 65, 12, 4147-4150, doi:10.1029/JZ065i012p04147.

Herrmann, R. B. (1985). An extension of random vibration theory estimates of strong ground motion to large distances, Bull. Seismol. Soc. Am., 75, 1447-1453, doi:10.1785/BSSA0750051447.

Hirn, A., M. Sapin, F. Ferrucci and G. Wittlinger (1991). Seismic heterogeneity of Mt. Etna: structure and activity, Geophys. J. Int., 105, 139-153, doi:10.1111/j.1365-246X.1991.tb03450.x.

Husid, L. R. (1969). Caracteristicas de Terremotos. Analisis General, Revista del IDIEM, 8, Santiago de Chile, 21-42.

Langer, H., G. Tusa, L. Scarfì and R. Azzaro (2016). Ground-motion scenarios on Mt. Etna inferred from empirical relations and synthetic simulations, Bull. Earthq. Eng., 14, doi:10.1007/s10518-015-9823-1.

Magri, L., M. Mucciarelli and D. Albarello (1994). Estimates of site seismicity rates using ill-defined macroseismic data, Pure Appl. Geophys. Pageoph., 143, 4, 617-632, doi:10.1007/bf00879501.

Meroni, F., G. Zonno, R. Azzaro, S. D'Amico et al. (2016). The role of the urban system dysfunction in the assessment of seismic risk in the Mt. Etna area (Italy), Bull. Earthq. Eng.,14, 7, doi:10.1007/s10518-015-9780-8.

Motazedian, D. and G. M. Atkinson (2005). Stochastic Finite-Fault Modeling Based on a Dynamic Corner Frequency, Bull. Seismol. Soc. Am., 95, 3, 995-1010, doi:10.1785/0120030207.

Peruzza, L., R. Azzaro, R. Gee, S. D'Amico et al. (2017). When probabilistic seismic hazard climbs volcanoes: the Mt. Etna case, Italy – Part 2: Computational implementation and first results, Nat. Hazards Earth Sys. Sci., 17, 11, 1999-2015, doi:10.5194/nhess-17-1999-2017.

Pessina, V., A. Garcia, F. Meroni, L. Sandri et al. (2023). From Multi-Hazard to Multi-Risk at Mount Etna: Approaches and Strategies of the PANACEA Project, in Advances in Natural Hazards and Volcanic Risks: Shaping a Sustainable Future, Malheiro A., F. Fernandes and H. I. Chaminé (Editors), Springer Nature Switzerland, Cham, Adv. Sci. Technol. Innov., 37-40, doi:10.1007/978-3-031-25042-2_7.

Pessina, V., F. Meroni, R. Azzaro and S. D'Amico (2021). Applying Simulated Seismic Damage Scenarios in the Volcanic Region of Mount Etna (Sicily): A Case-Study From the MW 4.9, 2018 Earthquake, Front. Earth Sci. 9, 629184, doi:10.3389/feart.2021.629184.

Pessina, V., F. Meroni, E. Varini and M. Longoni (2024). Probabilistic risk analysis due to volcanic and seismic hazards, Ann. Geophys., 68, 1, doi:10.4401/ag-9175.

Rotondi, R., E. Varini and C. Brambilla (2016). Probabilistic modelling of macroseismic attenuation and forecast of damage scenarios, Bull. Earthq. Eng., 14, 7, 1777-1796, doi:10.1007/s10518-015-9781-7.

Saragoni, G. R. and F. C. Hart (1974). Simulation of artificial earthquake accelerograms, J. Earthq. Eng. Struct. Dyn., 2, 249-267, doi:10.1002/eqe.4290020305.

Saraò, A., L. Moratto, E. Giampiccolo and O. Cocina (2023). Moment magnitude for earthquakes in the Etna volcano area, Geophys. J. Int., 234, 2519-2533, doi:10.1093/gji/ggad257.

Scognamiglio, L., L. Malagnini and A. Akinci (2005). Ground motion scaling in Eastern Sicily, Italy, Bull. Seism. Soc. Am., 95, 568-578, doi:10.1785/0120030124.

Tusa, G., H. Langer and R. Azzaro (2020). Localizing ground motion models in volcanic terranes: Shallow events at Mt. Etna, Italy, revisited., Bull. Seism. Soc. Am., 110, 6, 2842-2861, doi:10.1785/0120190325.

Zonno, G., R. Rotondi and C. Brambilla (2009). Mining macroseismic fields to estimate the probability distribution of the intensity at site, Bull. Seism. Soc. Am., 95, 5, 2876-2892, doi:10.1785/0120090042.

***CORRESPONDING AUTHOR: Salvatore D'AMICO**,
Istituto Nazionale di Geofisica e Vulcanologia, Osservatorio Etneo, Catania, Italy
e-mail: salvatore.damico@ingv.it